

1 **Biomass Burning Aerosol Absorption Measurements with MODIS**
2 **Using the Critical Reflectance Method**

3
4

Zhu, L., J. V. Martins, L. A. Remer

5
6
7

Li Zhu

8 University of Maryland, Baltimore County, Department of Physics and Joint Center for Earth
9 Systems Technology, 1000 Hilltop Circle, Baltimore, MD, 21250

10 410-455-1986

11 zhuli1@umbc.edu

12
13

14 Vanderlei J. Martins

15 University of Maryland, Baltimore County, Department of Physics and Joint Center for Earth
16 Systems Technology, 1000 Hilltop Circle, Baltimore, MD, 21250

17 410-455-2764

18 martins@umbc.edu

19
20

21 Lorraine A. Remer

22 code 613.2, NASA Goddard Space Flight Center, Greenbelt MD 20771 USA

23 301-614-6194

24 Lorraine.A.Remer@nasa.gov

25
26

27
28
29
30
31
32
33
34
35
36
37
38
39
40
41
42
43
44
45
46

Abstract

This research uses the critical reflectance technique, a space-based remote sensing method, to measure the spatial distribution of aerosol absorption properties over land. Choosing two regions dominated by biomass burning aerosols, a series of sensitivity studies were undertaken to analyze the potential limitations of this method for the type of aerosol to be encountered in the selected study areas, and to show that the retrieved results are relatively insensitive to uncertainties in the assumptions used in the retrieval of smoke aerosol. The critical reflectance technique is then applied to Moderate Resolution Imaging Spectrometer (MODIS) data to retrieve the spectral aerosol single scattering albedo (SSA) in South African and South American biomass burning events. The retrieved results were validated with collocated Aerosol Robotic Network (AERONET) retrievals. One standard deviation of mean MODIS retrievals match AERONET products to within ± 0.03 , the magnitude of the AERONET uncertainty. The overlap of the two retrievals increases to 88%, allowing for measurement variance in the MODIS retrievals as well. The ensemble average of MODIS-derived SSA for the Amazon forest station is 0.92 at 670 nm, and 0.84-0.89 for the southern African savanna stations. The critical reflectance technique allows evaluation of the spatial variability of SSA, and shows that SSA in South America exhibits higher spatial variation than in South Africa. The accuracy of the retrieved aerosol SSA from MODIS data indicates that this product can help to better understand how aerosols affect the regional and global climate.

I. Introduction

47
48
49 Atmospheric aerosols absorb solar radiation, warm the atmosphere (Penner et al., 1992), and
50 cool the Earth surface (Ramanathan et al., 2001). Therefore, they disturb the atmospheric
51 temperature profile (Ackerman et al., 2000; Ramanathan et al., 2007; Davidi et al., 2009), and
52 affect cloud properties (Koren et al., 2004; Koren et al., 2008; Feingold et al., 2005) and
53 precipitation (Ramanathan et al., 2001; Ramanathan et al., 2005; Menon et al., 2002). These
54 effects are particularly important over areas with high aerosol concentration (Sato et al, 2003;
55 Wang et al., 2004), such as the southern Africa region (Ichoku et al., 2003), the Amazon region
56 (Procopio et al., 2004), the Asian region (Ramana & Ramanathan, 2006), and Yellow Sea,
57 Arabian Sea, and Saharan Coast region (Zhu et al., 2007). A quantitative understanding of the
58 role of absorbing aerosols in climate change is also required to formulate reliable policy
59 recommendations (Hansen et al., 2000).

60 Aerosol absorption is typically expressed in terms of aerosol single scattering albedo
61 ($SSA = \frac{\text{aerosol scattering coefficient}}{\text{aerosol scattering coefficient} + \text{aerosol absorption coefficient}}$). The importance of
62 aerosol SSA to climate modification was first studied back in the 1970s (Atwater, 1970; Mitchell
63 JR, 1971). However, even though SSA is the biggest contributor to the total uncertainty in
64 aerosol direct radiative forcing (McComiskey et al., 2008), accurate aerosol SSA retrieval
65 remains challenging still today (Heintzenberg et al., 1997; Moosmuller et al., 2009). Many
66 approaches have been developed to study aerosol absorption properties, including microphysical
67 simulations (Ackerman & Toon, 1981; Martins, et al., 1998), data analysis from AERONET
68 (Dubovik et al., 2002), and in situ measurements (Clarke, et al., 1987; Reid, et al., 1998; Bond et al.,
69 1999; Martins, et al., 2009), and ground based remote sensing techniques (Dubovik et al., 1998).

70 Space based remote sensing techniques to measure aerosol absorption have also been
71 increasingly developed. More specifically, TOMS and combination of multi sensors on different
72 satellites have been used to study aerosol absorption. However, the retrieval of SSA from TOMS
73 is limited in the UV range (320-440nm), and the result is sensitive to the assumed aerosol layer
74 height (Herman, et al., 1997; Torres, et al., 1998). Moreover, the combination of satellite sensors,
75 such as TOMS and ERBE (Hus, et al., 2000), TOMS and MODIS (Hu, et al., 2007), OMI and
76 MODIS (Satheesh, et al., 2009), TOMS, MODIS and MISR (Hu, et al., 2009), and A-train
77 satellite sensors (MODIS, OMI, and CALIPSO) (Jeong & Hsu, 2008), have been used to retrieve
78 SSA. Nevertheless, these retrievals are still limited to the UV range, and the error sources
79 introduced by using multi platforms with different resolutions, slightly different observation
80 times, and different calibrations have not yet been well studied.

81 Recently, some other space based techniques have been proposed to study aerosol absorption as
82 well. Measuring aerosol SSA over ocean from space, by using ocean sun glint as a bright
83 background against aerosol absorption, was proposed by Kaufman, et al., in 2002. MISR also
84 has the ability to distinguish weakly absorbing (having 1%-4% of hematite, SSA in the range of
85 0.98-0.99) and strongly absorbing (having 10% hematite, red channel SSA of about 0.94) dust
86 components (Kalashnikova, et al., 2005; Kalashnikova, et al., 2006). Moreover, based on the
87 fact of differing sensitivities of polarized and unpolarized reflectance to aerosol absorption,
88 Glory will be used to retrieve SSA from polarimetric measurements in a single pixel
89 (Mishchenko, et al., 2007, Table 2). Even with these efforts, however, aerosol absorption
90 measurement with satellite remote sensing still remains challenging and more studies are needed.

91 Compared with the techniques discussed above, the “critical reflectance” method is also a
92 promising space based remote sensing technique to retrieve SSA (Fraser & Kaufman, 1985).

93 According to the Fraser and Kaufman (1985) radiative transfer simulations, there exists a
94 specific surface reflectance for which increased aerosol loading (being represented here by
95 aerosol optical depth or AOD) does not change the reflectance at the TOA (top of the
96 atmosphere). This unchanging reflectance at the TOA is defined as the critical reflectance, which
97 has a one-to-one relationship to aerosol SSA (Fraser & Kaufman, 1985). This technique has been
98 utilized with several space based remote sensing instruments to retrieve aerosol SSA: (1) using
99 Landsat Multi-Spectral Sensor Imagery as well as aircraft radiance data to retrieve aerosol SSA
100 over the DC area (Kaufman, 1987); (2) using AVHRR images in visible and near-IR bands to
101 retrieve the SSA of forest smoke (Kaufman, et al., 1990); (3) using Landsat TM images to
102 retrieve dust SSA, where the result agreed well with AERONET SSA (Kaufman, et al., 2001).

103 This research applies the critical reflectance technique to MODIS data to retrieve aerosol SSA.
104 The first MODIS sensor aboard NASA's Terra satellite was launched in 1999 and the second one
105 on the Aqua satellite launched in 2002. Each MODIS sensor provides a global data set every 1-2
106 days with a 16-day repeat cycle. The sensors collect the Earth images at 36 spectral bands in the
107 wavelength range from 0.4 μm to 14.4 μm with a swath width of 2330 km (cross track) and
108 continuous along-track coverage. Specifically, the seven aerosol bands are: 0.62-0.67, 0.84-0.87,
109 0.46-0.48, 0.55-0.57, 1.2-1.3, 1.63-1.65, and 2.11-2.16 μm , nominally 0.67, 0.86, 0.47, 0.55,
110 1.24, 1.64, and 2.12 μm respectively. This research discusses how to calculate the critical
111 reflectance from MODIS data and the sensitivity of potential factors affecting the retrieval, such
112 as detector zenith angle (DZA) and AOD difference between the polluted day and the clean days.
113 We also present validation results with collocated AERONET measurements as well as regional
114 SSA maps.

115

116

II. Calculating Critical Reflectance from MODIS Data

117

118

119

120

121

122

123

124

125

126

In this section, we use two days of MODIS images 16 days apart at the AERONET Mongu site (latitude= -15.25° , longitude= 23.15°) with low AOD (0.36 at $0.67 \mu\text{m}$) day 266 and high AOD (0.7 at $0.67 \mu\text{m}$) day 250 in year 2000 to describe how to calculate the critical reflectance parameter. The 16 days apart are used to assume the same angular geometry. In the rest of this study, we will refer to the low AOD day as the “clean day” and the high AOD day as the “polluted day”. Figure 1 shows the RGB images of the southern African region on the clean day (the image on the left) and the polluted day (the image on the right). Next, a 60×60 km area (latitude= $[-15.545$ to $-14.95]$; longitude= $[22.85$ to $23.45]$; blue color box in the image on the left and the purple color box in the image on the right) centered at Mongu is selected for detailed illustration.

127

128

129

130

131

Prior to the calculation of the critical reflectance, the cloud mask algorithm by Martins, et al. (2002) is applied to MODIS level 1B calibrated reflectance data (0.5 km resolution). After being projected on the grid of 100 pixels per degree (approximately 1 km resolution), the results on both days in the 60×60 km range are mapped in Fig. 2.

132

133

134

135

136

137

Next, the 3600 (60×60) pixels from both images in Fig. 2 are evenly divided into a 3×3 matrix to produce nine cells with equal numbers of 400 (20×20) pixels each. Then, using a scatter plot such as shown in Fig. 3 (showing the data from the first cell), we compare the reflectance from pixels in every cell on day 266 to each corresponding pixel on day 250. These data points are then fitted with a robust fit technique (the red color line in Fig. 3; DuMouchel & O'Brien, 1989), which minimizes the effect of potential outlier points. The corresponding

138 reflectance at the TOA that represents the crossing point between the fitted red line and the $y=x$
139 black line is by definition the critical reflectance. The intercept of the fitted red color line on the
140 y-axis is defined as the effective path radiance. Our radiative transfer simulations showed that
141 the effective path radiance is approximately 10 times the AOD difference between the clean day
142 and the polluted day. This result will be used later in the section describing the aerosol SSA
143 retrieval.

144

145 **III. Sensitivity Studies**

146

147 Aerosol SSA can be retrieved from the measured critical reflectance by inputting aerosol models
148 (aerosol size distribution and the real part of aerosol refractive index) on a Mie code (Wiscombe,
149 1980) and on a radiative transfer model (Santa Barbara DISORT Atmospheric Radiative Transfer
150 - SBDART by Ricchiuzzi, et al., 1998). To better understand this application and assess the
151 quality of the aerosol SSA retrieval results, we developed a series of sensitivity tests and
152 validated the results with collocated AERONET measurements. In the following sections, we
153 show these tests and validation outcomes, discuss factors affecting the retrieval results, and
154 display SSA maps.

155

156 Aerosol SSA can be retrieved through its unique correlation with the measured critical
157 reflectance. This technique has the distinct advantages of possible global coverage over land,
158 daily measurements, and the no need to know the Earth surface reflectance. It also carries the
159 following potential limitations: (a) it requires reasonable knowledge of the involved aerosol
160 models, (b) the critical reflectance should be AOD independent, (c) background aerosols on the
161 clean day and aerosols on the polluted day should have the similar SSA, (d) the Earth surface
162 must exhibit Lambertian reflectance, and (e) there needs to be a large enough AOD difference

163 between these two days. There are other limitations as well, such as the studied area should have
164 enough surface reflectance variability, aerosols should be homogeneously distributed within the
165 studied cell range, and the surface reflectance should be the same on the clean day and the
166 polluted day. In order to understand the importance of these limitations, a series of sensitivity
167 studies have been completed as shown in the following sub sections.

168 In addition, to study these sensitivities and validate aerosol SSA retrieved from MODIS, we have
169 to use other available column aerosol SSA measurements. Furthermore, high accuracy of aerosol
170 SSA - e.g. SSA uncertainty of 0.01 - is required to make accurate climatic predications.
171 However, the availability of aerosol SSA measurements qualifying these two conditions is
172 significantly limited. The Glory mission (to be launched in November 2010) by NASA might
173 improve this situation in the future. At present, we use AERONET measurements, in which
174 aerosol SSA uncertainty is 0.03 when AOD (at 440 nm) is greater than 0.4 (Dubovik et al.,
175 2004), for our validation. To be consistent, we compare the uncertainty caused by each
176 corresponding limitation also with 0.03, even though our goal is to measure aerosol SSA with
177 much smaller uncertainty. If the difference is significantly smaller than 0.03, we regard that the
178 limitation has little effect on the retrieved aerosol SSA and the uncertainty is acceptable; in
179 contrast, if the difference is greater than 0.03, it indicates that the limitation significantly affects
180 the aerosol SSA retrieval and needs to be considered in the retrieval algorithm.

181

182 **(a) Aerosol Models**

183

184 Aerosol models including aerosol size distribution and the real part of aerosol refractive index
185 from the research by Dubovik et al (2002) are used here as a first guess in our SSA retrieval.

186 These aerosol models are generated from AERONET data before 2000; however, MODIS

187 provides data after 2000. To see whether the models can represent the data from the years after
188 2000, the real part of aerosol refractive index is studied, and the result shows that the mean real
189 part of the refractive index for biomass burning aerosols over Mongu is 1.51, which agrees well
190 with the value of 1.51 from Dubovik et al's model (Dubovik, et al., 2002, table 1). Similar
191 comparisons over other AERONET sites also show good agreements between the data before
192 and after 2000. Therefore, Dubovik et al's aerosol models are used in our research to represent
193 the aerosol properties.

194 In addition, the data analysis shows that the ratio of its standard deviation of the real refractive
195 index over its mean value is approximately 2.3% over Mongu. The sensitivity study in Fig. 4
196 indicates that the 2.3% variation of the mean for a mean value of 1.495 (the real refractive index
197 from AERONET retrieval over Mongu on day 250 in year 2000) leads to an aerosol SSA
198 uncertainty of 0.01, 0.017, and 0.021 (with the imaginary refractive index as 0.012, 0.024, and
199 0.036 respectively, where 0.024 is the AERONET retrieved imaginary refractive index). This is
200 an acceptable uncertainty compared to the AERONET 0.03 error. This analysis indicates that the
201 sensitivity to real refractive index is relatively small and a relatively coarse first guess is
202 acceptable.

203

204

205 **(b) Dependence of Critical Reflectance on AOD**

206 The definition of critical reflectance assumes it to be AOD independent (Fraser & Kaufman,
207 1985, Figure 2). Nevertheless, a closer look at the crossing point shows that the simulated lines
208 cross each other in the neighborhood of one point, instead of exactly at that point (Kaufman,
209 1987), which implies that critical reflectance is weakly dependent on AOD. A sensitivity study to
210 determine the importance of this effect was performed. According to Fig. 5, when AOD on the

211 polluted day increases from 0.5 to 1.0 and AOD on the clean day remains as 0.1, the variation of
212 the critical reflectance is 0.01. This extreme case with the uncertainty of AOD between 0.5 to 1.0
213 leads to an SSA uncertainty of ± 0.0125 (at SSA=0.8) and ± 0.005 (at SSA=0.95), as in Fig.6.,
214 which are both significantly smaller than the 0.03 uncertainty from AERONET. In reality, we
215 will have a much better handle on the AOD uncertainties and will significantly reduce these error
216 bars.

217
218
219

(c) Varying Aerosol SSA on the Clean Day and on the Polluted Day

220 The basic critical reflectance technique also assumes that the background aerosols in both clean
221 days and polluted days have the same SSA. However, this condition might not be satisfied. To
222 study how aerosol SSA variation affects the retrieval results, we assume that on the polluted day
223 aerosol SSA (at 0.67 μm) is 0.898 and AOD is 0.7, on the clean day AOD is 0.2 and SSA (on
224 clean day) varies from 0.986 to 0.824 as in column 2 of Table. 1. The results of a similar analysis
225 of SSA are also shown in Table 1: on the polluted day SSA is 0.972 and varies from 0.910 to
226 0.993 on the clean day. The real part refractive index is kept at 1.51 for both days. The results in
227 column 5 of Table 1 show that the difference between the retrieved SSA and the SSA on the
228 polluted day varies between -0.026 to 0.019 (when SSA on the polluted day is 0.898) and -0.006
229 to 0.018 (when SSA on the polluted day is 0.972). Considering these differences are still smaller
230 than the AERONET aerosol SSA uncertainty 0.03 even under extreme cases, we regard that
231 varying the aerosol SSA between the clean day and the polluted day affects retrieved aerosol
232 SSA with acceptable uncertainty.

233
234
235
236

(d) DZA

237 The data analysis shows that detector zenith angle (DZA) affects retrieval results when it is
238 bigger than 40 degrees. This issue can be demonstrated through the results of a group of cases
239 over Senanga in 2000. According to Fig. 7, when DZA is greater than 40 degrees, the deviation
240 of MODIS SSA from AERONET SSA increases as DZA increases. In addition, in order to keep
241 the deviation below 0.03, DZA needs to be smaller than 40 degrees. This result is likely due to
242 the fact that our retrieval applies the simplified assumption of Lambertian Earth surface
243 reflectance, instead of the reflectance with angular distribution usually modeled by the Bi-
244 directional Reflectance Distribution Function (BRDF) (Maignan, et al., 2004). This issue will be
245 addressed in more detail in our future research with the incorporation of the Earth surface BRDF
246 in radiative transfer simulations. At this point, we will only select cases with $DZA < 40$ degrees
247 as a quality assurance procedure. The similar analysis of SSA with scattering angle and SSA
248 with solar zenith angle does not show SSA dependence on these two geometries as its
249 dependence on DZA.

250
251

252 (e) **AOD Difference between the Clean day and the Polluted Day**

253 Besides DZA, AOD difference (between the clean day and the polluted day) affects the signal to
254 noise ratio and hence the accuracy of the SSA retrieval. A group of cases over Mongu in 2000 is
255 used to study this issue. As shown in Fig.8, in order to keep the deviation of MODIS SSA from
256 AERONET SSA below 0.03, the AOD difference needs to be greater than 0.2 to have a high
257 enough signal to noise ratio.

258
259

260 In summary, these sensitivity studies concerning the aerosol model about the real part of aerosol
261 refractive index, AOD dependence of the critical reflectance, and variations of the aerosol SSA

262 between on the clean day and the polluted day show that the uncertainties of retrieved aerosol
263 SSA caused by these factors are acceptable for a satellite retrieval of aerosol SSA. In addition, to
264 produce retrieval results in good agreement with AERONET measurements, a case need to
265 satisfy two conditions: DZA is smaller than 40 degrees, and the AOD difference between clean
266 day and polluted day is bigger than 0.2.

267

268 **IV. Algorithm and Validation Strategy**

269 After doing sensitivity studies, we apply the critical reflectance technique on some cases of
270 MODIS data to retrieve aerosol SSA. Our studied regions are dominated by biomass burning
271 aerosols and are collocated with the AERONET sites as follows: Senanga (African savanna),
272 Mongu (African savanna), Mwinilunga (African savanna), and Alta Floresta (Amazon forest).
273 The studied cases are selected based on evaluating MODIS RGB images, MODIS data, and
274 AERONET data to determine that: (1) cloud cover is minimal over the study areas on both the
275 clean day and polluted day, 16 days apart; (2) MODIS DZA is less than 40 degrees; (3) these two
276 days have AOD difference (at 670 nm) greater than or equal to 0.2; and (4) AERONET has level
277 2 aerosol SSA retrievals available for the polluted day. All retrieval results are validated with
278 collocated AERONET retrieval products, and regional SSA maps are produced.

279 As discussed in section I, aerosol SSA can be retrieved from the critical reflectance
280 measurements performed with MODIS data as shown in Fig. 1, 2, and 3. Next, as quality control,
281 we have removed cells bearing any of the following properties: (1) having negative critical
282 reflectance; (2) SSA greater than 1 or smaller than 0; (3) an SSA uncertainty derived from robust
283 fitting (DuMouchel & O'Brien, 1989) greater than 0.03; (4) root mean square error (RMSE)

284 greater than 0.006 between the data points and the fitting results; and (5) the effective path
285 radiance smaller than 0.02 (corresponding to an AOD difference greater than 0.2).

286 In addition, recent studies have shown that aerosol SSA varies with biomass burning stages and
287 the aerosol aging process (Abel et al., 2003; Zaveri et al., 2010). Therefore, AERONET level 2
288 aerosol SSA measured at the closest time to the MODIS overpass time is used for the validation,
289 instead of the daily average. In these AERONET level 2 closest time SSA retrievals, the SZA is
290 in the range of 53 degrees to 76 degrees. We compare the AERONET SSA with the mean and
291 the standard deviation of our retrieved aerosol SSA. In order to calculate aerosol SSA variance
292 with less than nine samples, we apply a chi square distribution correction and set a confidence
293 interval of 50% (Bevington, 1969).

294
295 According to our quality assurance analysis, accurate biomass burning aerosol SSA can be
296 retrieved with the critical reflectance technique at 0.47, 0.55, and 0.67 μm channels; however,
297 there is not enough signal to noise ratio at the other four aerosol channels (0.86, 1.24, 1.64, and
298 2.12 μm) to retrieve biomass burning aerosol SSA, i.e., there are no cells left out of nine total
299 after applying our data quality criteria. Next, we validate aerosol SSA retrieved from MODIS
300 data with collocated AERONET measurements (AERONET SSAs at 0.47 and 0.55 μm used here
301 is the 1st order interpolation AERONET SSAs at 0.440 and 0.676 μm).

302

303

V. Results

304 (a) Aerosol SSA Measurements over 60×60 km Area

305 Aerosol SSA was retrieved by applying the algorithm described above, and the result was
306 compared with collocated AERONET measurements in South Africa and South America.

307 According to Fig. 9, approximately one standard deviation (68% by only considering the mean;

308 88% by considering the mean and the variance) of all the studied cases satisfies the requirement
309 that the absolute difference between MODIS SSA and AERONET SSA is smaller than 0.03.
310 Figure 9 also indicates that aerosol SSA has a larger spatial variation (represented by larger error
311 bars) in South America than in South Africa. Specifically, the mean value of the sample
312 variance is 0.04 for the cases in South America and 0.02 in South Africa.

313
314 In addition, the comparison of the mean and sample variance of aerosol SSA over time for each
315 studied locations between MODIS retrievals and AERONET measurements is displayed in
316 Table. 2. According to Table. 2, aerosol SSA retrievals from MODIS are biased lower than
317 AERONET measurements over Mwinilunga, which might be caused by problems in either
318 MODIS or AERONET retrievals. Table 2 also shows that climatologically for the other sites,
319 MODIS retrieval results agree well with AERONET measurements. The biggest difference
320 between MODIS mean and AERONET mean is 0.02. This indicates that aerosol SSA retrieved
321 from MODIS is accurate enough to be used in climatologic studies.

322
323 **(b) Regional Aerosol SSA Maps**

324 The above validation results show that applying the critical reflectance technique with MODIS
325 data can retrieve aerosol SSA in reasonable agreement with AERONET results within
326 AERONET uncertainty levels. Next, by expanding the studied areas, we produce regional
327 aerosol SSA maps, which have wide applications in climate modeling and radiative forcing
328 calculations. For example, Figure 10 and Figure 11 show aerosol SSA (at 470 nm) maps over
329 South Africa and South America. In addition, the means and the standard deviations
330 (representing the spatial variation) of aerosol SSA at 470, 550, and 670 nm over both regions are
331 listed in Table. 3. Again, these results also indicate that aerosol SSA has a larger spatial

332 variation in South America than in South Africa, which is in consistent with the results from Fig.
333 9. The SSA map over the Amazon shows significant connection between the distribution of SSA
334 and AOD. Both results (AOD and SSA) show greater values in the northern part of the Amazon,
335 which is compatible with the particle properties and aerosol loading of forest smoke versus and
336 Cerrado smoke (Dubovik et al., 2002).

337
338
339
340

VI. Conclusions

341 In this research, the critical reflectance technique is applied on MODIS data from biomass
342 burning regions by comparing reflectance at TOA in two days (a clean day and a polluted day 16
343 days apart) to retrieve the aerosol SSA on the polluted day. First, this study describes a method
344 to determine critical reflectance from MODIS data. Second, sensitivity studies that examine a
345 range of aerosol conditions expected for our study areas - about aerosol models, the variation of
346 the real part of aerosol refractive index, AOD dependence of the critical reflectance, and the
347 variation of background aerosol SSA between a clean day and a polluted day – indicate that these
348 factors have manageable effect on the retrieval results. In the mean time, a DZA smaller than 40
349 degrees and an AOD difference greater than 0.2 are required to provide accurate retrieved
350 aerosol SSA values. We did not test the effect of our assumptions of particle size and shape on
351 retrievals of SSA because the all smoke aerosol is expected to be spherical and with minimal
352 variation in size distribution. Critical reflectance retrievals and subsequent mapping to SSA may
353 show greater sensitivities and uncertainties for other aerosol types and different surfaces.
354 Aerosol mixtures of smoke and dust may be especially difficult.

355 Validation results show that the retrieved aerosol SSA from MODIS agrees well with collocated
356 AERONET measurements. The ensemble average SSA results from the critical reflectance

357 techniques are in good agreement with collocated AERONET ensemble averages, within 0.02 in
358 all cases, except for the Mwinilunga station that seems to present some artificial bias.
359 Moreover, the analysis of aerosol SSA from MODIS retrievals concludes that aerosol SSA has a
360 larger spatial variation in South America than in South Africa, and that we can see the South
361 American north-south gradient in SSA and AOD reported by previous studies. Likewise the
362 critical reflectance method also reproduces findings that show African savanna SSA about 0.08
363 to 0.09 lower than what is measured in the Amazon forest.

364 However, the power of the critical reflectance method is not in its ability to reproduce previous
365 point measurements or retrievals, either spatially (AERONET) or temporally (field experiments).
366 The true contribution of the critical reflectance method, demonstrated here, is to offer frequent
367 quantitative measures of spectral aerosol SSA over broad regions, and to capture the spatial and
368 temporal variability of this essential particle property.

369

370 **Acknowledgements.** We would like to thank NASA for funding this project with under the grant
371 NNX08AJ78G. We also would like to thank the MODIS team and AERONET team for their excellent
372 work on the instrument development, maintenance, and calibration. We thank their effort on data quality
373 control and providing data to the public as well. Thanks also go to Kelley Wells, Tom Eck, TianLe Yuan,
374 and Ralph Kahn for many helpful comments.

375

376 **References:**

- 377 Ackerman, A.S., Toon, O.B., Stevens, D.E., Heymsfield, A.J., Ramanathan, V., & Welton, E.J.
378 (2000). Reduction of Tropical Cloudiness by soot. *Science*, Vol. 288, No. 5468, pp. 1042-1047.
- 379 Ackerman, T.P., & Toon, O.B. (1981). Absorption of visible radiation in atmosphere containing
380 mixtures of absorbing and nonabsorbing particles. *Applied Optics*, Vol. 20, No. 20, pp. 3661-
381 3668.
- 382 Atwater, M.A. (1970). Planetary Albedo Changes Due to Aerosols, *Science*, Vol. 170, No 3953,
383 pp. 64-66.
- 384 Bevington, P.R. (1969). Data reduction and error analysis for the physical sciences. New York: McGraw-
385 Hill.
- 386 Bond, T. C., Anderson, T. L., & Campbell, D. (1999) Calibration and inter comparison of filter-based
387 measurements of visible light absorption by aerosols, *Aerosol Sci Tech*, Vol. 30, pp. 582-600.
- 388 Clarke, A.D., Noone, K.J., Heintzenberg, J., Warren, S.G., & Covert, D.S. (1987). Aerosol light absorption
389 measurement techniques: analysis and intercomparisons. *Atmospheric Environment*, Vol. 21, No. 6, pp.
390 1455-1465.
- 391 Davidi, A., Koren, I., & Remer, L. (2009). Direct measurements of the effect of biomass burning
392 over the Amazon on the atmospheric temperature profile. *ACPD*, Vol. 9, pp. 12007-12025.
- 393 Dubovik O, Holben, B.O., Lapyonok, T., Sinyuk, A, Mishchenko, I, Yang, P., et al (2002). Non
394 spherical aerosol retrieval method employing light scattering by spheroids. *Geophys Res Lett*,
395 Vol. 29, NO. 10, 10.1029/2001GL014506
- 396 Dubovik, O., Holben, B.N., Kaufman, Y.J., Yamasoe, M., Smirnov, A., & Tanre, D., et al. (1998).
397 Single-scattering albedo of smoke retrieved from the sky radiance and solar transmittance
398 measured from ground. *J. Geophys. Res.*, Vol. 103, No. D24, pp. 31,903-31,923.

399 DuMouchel, W. H., & F. L. O'Brien (1989). Integrating a robust option into a multiple
400 regression computing environment. *Computer Science and Statistics: Proceedings of the 21st*
401 *Symposium on the Interface*. Alexandria, VA: American Statistical Association.

402 Feingold,G., Jiang,H., & Harrington, J.Y. (2005). On smoke suppression of clouds in Amazonia,
403 *Geophys Res Lett*, Vol.32, L02804, doi: 10.1029/2004GL021369.

404 Fraser,R.S. & Kaufman, Y. J. (1985). The relative importance of Aerosol Scattering and
405 Aabsorption in Remote Sensing. *IEEE TRANSACTIONS ON GEOSCIENCE AND REMOTE*
406 *SENSING*, Vol. GE-23, No.5, pp. 625-633.

407 Hansen, A.D.A., Rosen, H., & Novakov, T. (1984). The aethalometer-an instrument for the real -
408 time measurement of optical absorption by aerosol particles. *Sci Total Environ*, Vol.36, pp. 191-
409 196.

410 Hansen,J., Sato,M., Ruedy, R., Lacis, A., & Oinas, V. (2000). Global warming in the twenty-first
411 century: an alternative scenario. *PNAS*, Vol. 97, Part. 18, pp 9875-9880.

412 Herman,R.J.,Bhartia,K.P., Torres,O., Hsu,C., Seftor,C., & Celarier,E. (1997). Global distribution
413 of UV-absorbing aerosols from Nimbus 7/TOMS data. *J. Geophys. Res.*, Vol. 102, No. D14, pp.
414 16911-16922.

415 Hsu, N. C., J. R. Herman, and C. Weaver (2000), Determination of radiative forcing of Saharan
416 dust using combined TOMS and ERBE data, *J. Geophys. Res.*, 105(D16), 20,649-20,661.

417 Hu, R.M., Martins, R.V., & Fairlie, T.D. (2007). Global retrieval of columnar aerosol single
418 scattering albedo from space-based observations. *J. Geophys. Res.*, Vol. 112, D02204, doi:
419 10.1029/2005JD006832.

420 Hu, R.M., Sokhi, R.S., & Fisher, B.E.A. (2009). New algorithms and their application for
421 satellite remote sensing of surface PM_{2.5} and aerosol absorption. *Aerosol Science*, Vol. 40, pp.
422 394-402.

423 Ichoku, C., Remer, L.A., Kaufman, Y.J., Levy, R., Chu, D.A., & Tanre, D., et al. (2003). MODIS
424 observation of aerosols and estimation of aerosol radiative forcing over southern Africa during
425 SAFARI 2000. *J. Geophys. Res.*, Vol. 108, No. D13, pp. 8499-8511.

426 Jeong, M-J., & Hsu, N. C. (2008). Retrievals of aerosol single-scattering albedo and effective
427 aerosol layer height for biomass-burning smoke: Synergy derived from "A-Train" sensors.
428 *Geophys Res Lett*, Vol. 35, L24801, doi: 10.1029/2008GL036279.

429 Kalashnikova, O.V., Kahn, R., Sokolik, I.N., & Li, W-H. (2005). Ability of multiangle remote
430 sensing observations to identify and distinguish mineral dust types: Optical models and retrievals
431 of optically thick plumes. *J. Geophys. Res.*, Vol. 110, D18S14, doi:10.1029/2004JD004550.

432 Kalashnikova, O.V., & Kahn, R., (2006). Ability of multiangle remote sensing observations to
433 identify and distinguish mineral dust types: 2. Sensitivity over dark water. *J. Geophys. Res.*, Vol.
434 111, D11207, doi:10.1029/2005JD006756.

435 Mishchenko, M.I., Cairns, B., Kopp, G., Schueler, C.F., Fafaul, B.A., & Hansen, J.E., et al.
436 (2007). Accurate Monitoring of Terrestrial Aerosols and Total Solar Irradiance- Introducing the
437 Glory Mission. *American Meteorological Society*, pp. 677-691.

438 Kaufman, Y. J. (1987). Satellite Sensing of Aerosol Absorption. *Journal of Geophysical*
439 *Research*, Vol. 92, No.D4, pp. 4307-4317.

440 Kaufman, Y.J., Tucker, C.J., & Fung, I. (1990). Satellite Measurements of Large-Scale Air
441 Pollution: Methods. *J. Geophys. Res.*, Vol. 95, No.D7, pp. 9927-9939.

442 Kaufman, Y.J., Tanre, D., Dubovik, O., Karnieli, & Remer, L.A. (2001). Absorption of sunlight by
443 dust as inferred from satellite and ground-based remote sensing. *Geophys Res Lett*, Vol. 28, No.
444 8, pp. 1479-1482.

445 Kaufman, Y.J., Tanre, D., & Boucher, O. (2002). A satellite view of aerosols in the climate
446 system. *Nature*, Vol 419, pp. 215-223.

447 Koren, I., Kaufman, Y.J., Remer, L.A., & Martins, J.V. (2004). Measurements of the effect of
448 Amazon Smoke on inhibition of Cloud Formation. *Science*, Vol. 303, No. 5662, pp. 1342-1345.

449 Koren, I., Martins, J.V., Remer, L.A., & Afargan, H. (2008). Smoke invigoration versus inhibition
450 of clouds over the Amazon. *Science*, Vol. 321, pp. 946-949.

451 Martins, J. V., Artaxo, P., Liousse, C., Reid, J. S., Hobbs, P. V., & Kaufman Y. J. (1998), Effects of
452 black carbon content, particle size, and mixing on light absorption by aerosols from biomass burning in
453 Brazil, *J. Geophys. Res.*, 103(D24), 32,041–32,050, doi:10.1029/98JD02593.

454 Martins, J. V., Didier, T., Remer, L., Kaufman, Y., Mattoo, S., & Levy, R., (2002). MODIS cloud
455 screening for remote sensing of aerosols over oceans using spatial variability : First result and evaluation
456 of aerosol from the Terra Spacecraft (MODIS). *Geophys Res Lett*, Vol. 29, No. 12,
457 10.1029/2001GL013252.

458 Martins, J. V., Artaxo, P., Kaufman, Y.J., Castanho, A.D., & Remer, L.A. (2009). Spectral
459 absorption properties of aerosol particles from 350-2500nm. *Geophys Res Lett*, Vol. 36, L13810.

460 McComiskey, S. E. Schwartz, B. Schmid, H. Guan, E. R. Lewis, P. Ricchiazzi, and J. A. Ogren
461 (2008), Direct aerosol forcing: Calculation from observables and sensitivities to inputs, *J.*
462 *Geophys. Res.*, 113, D09202, doi:10.1029/2007JD009170.

463 Mitchell, J.M.J.R. (1971). The Effect of Atmospheric Aerosols on Climate with Special Reference to
464 Temperature near Earth's surface. *Journal of Applied Meteorology*, Vol. 10, Issue. 4, pp. 703-714.

465 Moosmuller, H., Chakrabarty,P.K., & Arnott,W.P. (2009). Aerosol Absorption and its
466 measurement: A review. *Journal of Quantitative Spectroscopy and Radiative Transfer*, Vol.110,
467 issue. 11, pp. 844-878.

468 Penner, J.E., Dickinson,E.R., & O'Neill, A.C. (1992). Effects of aerosol from Biomass burning
469 on the global radiation budget. *Science*, Vol.256, No.5062, pp. 1432-1434.

470 Ramana,M.V. & Ramanathan,V. (2006). Abrupt transition from natural to anthropogenic aerosol
471 radiative forcing: observations at the ABC-Maldives Climate Observatory. *J. Geophys. Res.*,
472 Vol. 111, D20207, doi:10.1029/2006JD007063

473 Ramanathan, V., Ramana,M.V., Roberts, G., Kim, D., Corrigan, C., & Chung, C., et al. (2007).
474 *Nature*, Vol. 448, pp. 575-579.

475 Ramanathan, V., Chung, C., Kim, D., Bettge,T., Buja,L., & Kiehl,J.T., et al. (2005). Atmospheric
476 brown clouds: impacts on South Asian climate and hydrological cycle. *PNAS*, Vol. 102, No. 15,
477 pp. 5326- 5333.

478 Ramanathan, V., Crutzen, P.J., Kiehl,J.T., & Rosenfeld, D. (2001) . Aerosols,climate,and the
479 hydrological cycle. *Science*, Vol. 294, pp. 2119-2124.

480 Reid, J. S., Hobbs, P. V., Liousse, C., Martins, J. V., Weiss, R. E., & Eck, T. F.(1998).
481 Comparisons of techniques for measuring shortwave absorption and black carbon content of
482 aerosols from biomass burning in Brazil, *J. Geophys. Res.*, 103(D24), pp. 32,031-32,040.

483 Satheesh, S. K., Torres,O., Remer,L.A., Babu,S.S., Vinoj, V. & Eck,T.F., et al. (2009).
484 Improved assessment of aerosol absorption using OMI-MODIS joint retrieval, *J. Geophys. Res.*,
485 Vol. 114, D05209, doi:10.1029/2008JD011024.

486 Sato, M., Hansen,J., Koch,D., Lacis,A., Ruedy, R., & Dubovik, O, et al. (2003). Global
487 atmospheric black carbon inferred from AERONET. *PNAS*, Vol. 100, No. 11, pp. 6319-6324.

488 Torres, O., P. K. Bhartia, J. R. Herman, Z. Ahmad, and J. Gleason (1998), Derivation of aerosol
489 properties from satellite measurements of backscattered ultraviolet radiation: Theoretical basis, *J.*
490 *Geophys. Res.*, 103(D14), 17,099-17,110.

491 Wang, C. (2004). A modeling study on the climate impacts of black carbon aerosols. *J. Geophys.*
492 *Res.*, Vol. 109, D03106, doi: 10.1029/2003JD004084.

493 Zhu, A, V.Ramanathan, F.Li & D.Kim (2007), Dust plumes over the Pacific, Indian, and
494 Atlantic oceans: Climatology and radiative impact, *J.Geophys.Res.*, 112, D16208,
495 doi:10.1029/2007JD008427.

496 **Figure captions:**

497 **FIG.1.** MODIS RGB images over Africa. The image on the left is for Julian day 266 of year
498 2000 (clean day), and the blue color box in it represents the 60×60 km region around the
499 AERONET site Mongu. Likewise, the image on the right is for day 250 of year 2000 (polluted
500 day), and the purple color box represents the same 60×60 km region as the blue color box on
501 the left image. The blue color box and purple color box are used respectively to contrast the
502 clean day and the polluted day.

503 **FIG.2.** Projected apparent reflectance for the polluted and clean day at 670 nm after applying a
504 common cloud mask to both days. The image on the left shows the reflectance in the blue color
505 box in Fig.1 with an average AOD (at 670 nm) =0.36. The image on the right shows the
506 reflectance in the purple color box in Fig.1 with an averaged AOD (at 670 nm) =0.7. The color
507 bar represents the apparent reflectance.

508 **FIG.3.** This figure demonstrates how to calculate critical reflectance using MODIS data from
509 two days. The blue dots are the scatter plot of the reflectance from the first cell (20×20 km
510 range) on the polluted day (the y-axis) versus that on the clean day (the x-axis). The red color
511 line represents the robust fit of the data. The black color line represents $y=x$, when reflectance
512 (at the TOA) on the clean day equals reflectance (at the TOA) on the polluted day. The
513 reflectance value at the crossing point (as shown by the arrows in the figure) between the black
514 color line and the red color line is defined as “critical reflectance”. The intercept of the fitted red
515 color line on the y- axis is defined as “effective path radiance”.

516 **FIG.4.** Sensitivity study for the variation of the real part of aerosol refractive index. The x- axis
517 represents the real part of the refractive index, and the y-axis represents aerosol SSA calculated

518 from Mie theory. The real refractive index as 1.49, the imaginary refractive index as 0.024, and
519 the input size distribution are from AERONET retrieval results over Mongu on day 250 in year
520 2000. This result shows that an uncertainty of real part of aerosol refractive index of 2.3% leads
521 to an SSA uncertainty of 0.01, 0.017, and 0.021 when the imaginary refractive index is 0.012,
522 0.024, and 0.036 respectively.

523 **FIG.5.** This figure shows the AOD dependence of the critical reflectance. The x-axis represents
524 AOD (at 670 nm) on a polluted day, and the y- axis represents the calculated critical reflectance
525 for AOD values (at 670 nm; on a clean day) of 0.1 (red solid line), 0.2 (green solid line), and 0.3
526 (continued light blue line). The simulations use the following conditions: solar zenith angle
527 (SZA)=26.8 degrees, solar azimuth angle (SAZA)=37.77 degrees, detector zenith angle
528 (DZA)=38.65 degrees, user azimuth angle (ϕ)=277.38 degrees, wavelength=0.67 μm , and
529 SSA=0.8. When AOD on the clean day varies from 0.1 to 0.3, the variation of critical reflectance
530 is 0.005 (AOD of 0.5 on polluted day) and 0.003 (AOD of 1 on polluted day). In addition, when
531 AOD on the polluted day varies from 0.5 to 1, the variation of critical reflectance is 0.01(AOD of
532 0.1 on the clean day).

533 **FIG.6.** The sensitivity study of aerosol SSA (at 670 nm) to varying critical reflectance. The x-
534 axis represents SSA, and the y-axis represents critical reflectance. The green curve shows the
535 unique correlation between critical reflectance and SSA. AOD on the clean (polluted day) day is
536 0.2 (0.7). It shows that the critical reflectance uncertainty of 0.01 leads to an SSA uncertainty of
537 0.025 (when SSA=0.8). Similarly, a critical reflectance uncertainty of 0.028 causes an SSA total
538 uncertainty of 0.01 (when SSA=0.95).

539 **FIG.7.** This figure demonstrates that DZA affects aerosol SSA retrievals. The x-axis represents
540 DZA for each case, and the y-axis represents the absolute difference between the retrieved
541 aerosol SSA (over Senanga in 2000) from MODIS on *TERRA* and AERONET level 2 daily-
542 averaged aerosol SSA. The red color bar over each data point represents the AERONET SSA
543 uncertainty of 0.03. The result indicates that the difference between aerosol SSA retrieved from
544 MODIS and from AERONET increases as DZA increases. This effect is likely caused by the
545 simplified assumption of a Lambertian surface reflectance in the radiative transfer simulations.

546 **FIG.8.** This figure demonstrates that AOD differences affect aerosol SSA retrievals. The x-axis
547 represents the AOD difference at 670 nm between the clean day and the polluted day, and the y-
548 axis represents the absolute difference between aerosol SSA (over Mongu in 2000) retrieved
549 from MODIS and AERONET level 2 daily-averaged aerosol SSA. The result shows that AOD
550 difference needs to be greater than 0.2 in order to produce a high enough signal to noise ratio and
551 to keep the deviation of MOIDS SSA from AERONET SSA below 0.03.

552 **FIG.9.** Comparison of aerosol SSA retrieved from MODIS with collocated AERONET
553 measurement in South Africa (plots on the left) and South America (plots on the right). The x-
554 axis represents the case numbers, and the y-axis represents the difference between aerosol SSA
555 from AERONET and from MODIS. In addition, bars over each data point represent SSA
556 variance (among the remaining cells in 60×60 km range) at a 50% of confidence interval and
557 with a chi square distribution correction. Since AERONET SSA has an uncertainty of 0.03, the
558 aerosol SSA retrieved from MODIS agrees well with AERONET measurements (68% by only
559 considering the mean; 88% by considering the mean and the variance), i.e., the absolute
560 difference between aerosol SSA from AERONET and MODIS is smaller than 0.03. The result
561 also shows that aerosol SSA has a larger spatial variation in South America than in South Africa.

562 **FIG. 10.** Regional AOD and aerosol SSA (at 470 nm) maps. The figures on the left represent the
563 region over South Africa with latitude = [-15 to -11] and longitude = [21 to 25] on day 254 in
564 2000 (day 238 as the clean day). The figures on the right represent the region over South
565 America with latitude = [-12 to -8] and longitude = [-60 to -56] on day 241 in 2006 (with 225 as
566 the clean day). Both images have a resolution of 20×20 km.

567 **FIG. 11.** Regional AOD and aerosol SSA (at 470 nm) maps. The figures on the left represent the
568 region over South Africa with latitude = [-18 to -14] and longitude = [22 to 26] on day 250 in
569 2000 (day 266 as the clean day). The figures on the right represent the region over South
570 America with latitude = [-16 to -12] and longitude = [-60 to -56] on day 252 in 2004 (with 268 as
571 the clean day). Both images have a resolution of 20×20 km.

572

573

574 Table. 1. Sensitivity study for varying aerosol SSA between the clean day and the polluted day.
575 Wavelength = 0.67 μm ; AOD (on clean day) = 0.2; AOD (on polluted day) = 0.7; SZA = 26.8°;
576 SAZA = 37.77°; DZA = 38.65°; DAZA = 277.38°; Real part of the refractive index = 1.51. The
577 first (last) four rows in the first column represents aerosol SSA on polluted day as a constant
578 0.898 (0.972); the second column represents varying aerosol SSA on clean day; the third column
579 represents the simulated critical reflectance; the fourth column represents the retrieved aerosol
580 SSA; and the last column is the difference between the retrieved aerosol SSA and the real aerosol
581 SSA on the polluted day. The results show that the uncertainty caused by varying aerosol SSA
582 between the clean day and the polluted day is acceptable.

583

SSA (on polluted day)	SSA (on clean day)	Critical reflectance	SSA (Retrieved)	SSA (retrieved) – SSA (polluted day)
0.898	0.986	0.205	0.872	-0.026
	0.934	0.226	0.887	-0.011
	0.855	0.263	0.909	0.011
	0.824	0.281	0.917	0.019
0.972	0.993	0.461	0.966	-0.006
	0.986	0.473	0.968	-0.004
	0.934	0.601	0.983	0.011
	0.910	0.691	0.990	0.018

587 Table 2. The mean and sample variance of aerosol SSA from MODIS retrievals and AERONET
 588 measurements over different locations. The table shows that MODIS retrievals are biased smaller
 589 than AERONET measurements over Mwinilunga, which might be caused by either problems in
 590 MODIS or in the AERONET retrievals. Over other sites, the maximum difference between
 591 MODIS SSA and AERONET SSA is 0.02. This high accuracy aerosol SSA retrievals from
 592 MODIS indicates its promising application in climatological studies over a given region.

593

AERONET sites	SSA (at 470 nm)		SSA (at 550 nm)		SSA (at 670 nm)	
	AERONET	MODIS	AERONET	MODIS	AERONET	MODIS
Alta Floresta	0.92 ± 0.02 (22 cases)	0.92 ± 0.03	0.91 ± 0.03 (22 cases)	0.92 ± 0.03	0.92 ± 0.03 (18 cases)	0.90 ± 0.03
Senanga	0.86 ± 0.01 (7 cases)	0.87 ± 0.01	0.85 ± 0.01 (7 cases)	0.87 ± 0.01	0.84 ± 0.01 (7 cases)	0.86 ± 0.01
Mongu	0.88 ± 0.02 (14 cases)	0.86 ± 0.02	0.87 ± 0.03 (14 cases)	0.86 ± 0.02	0.86 ± 0.03 (14 cases)	0.84 ± 0.02
Mwinilunga	0.90 ± 0.02 (3 cases)	0.86 ± 0.01	0.90 ± 0.02 (3 cases)	0.85 ± 0.01	0.89 ± 0.03 (3 cases)	0.84 ± 0.01

594

595

596 Table 3. This table shows the mean and the standard deviation of aerosol SSA at 470, 550, and
 597 670 nm for the same cases as shown in SSA maps in Fig. 10 and Fig. 11. The data in the table
 598 shows aerosol SSA has a larger spatial variation in South America than in South Africa, which is
 599 consistent with the result from Fig.9.

600

Case Information	Aerosol SSA: mean \pm standard deviation		
	470 nm	550 nm	670 nm
latitude = [-15 to -11]; longitude = [21 to 25] over South Africa; on day 254 in 2000	0.86 \pm 0.02	0.84 \pm 0.02	0.82 \pm 0.02
latitude=[-18 to -14]; longitude=[22 to 26] over South Africa; on day 250 in 2000	0.86 \pm 0.02	0.84 \pm 0.02	0.81 \pm 0.02
latitude =[-12 to -8]; longitude = [-60 to -56] over South America; on day 241 in 2006	0.90 \pm 0.03	0.90 \pm 0.03	0.87 \pm 0.04
latitude=[-16 to -12]; longitude=[-60 to -56] over South America; on day 252 in 2004	0.91 \pm 0.04	0.92 \pm 0.03	0.91 \pm 0.03

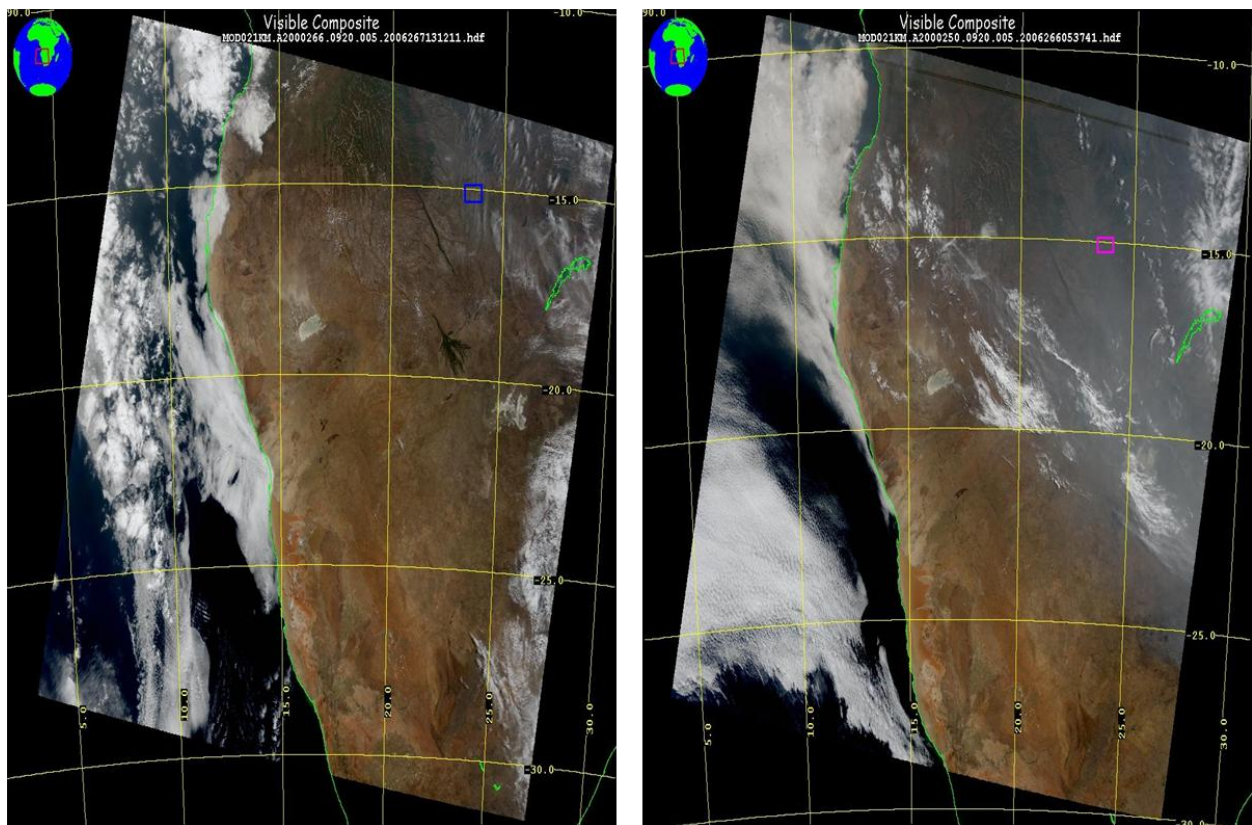
601

602

603

604 FIG.1. MODIS RGB images over Africa. The image on the left is for Julian day 266 of year
605 2000 (clean day), and the blue color box in it represents the 60×60 km region around the
606 AERONET site Mongu. Likewise, the image on the right is for day 250 of year 2000 (polluted
607 day), and the purple color box represents the same 60×60 km region as the blue color box on
608 the left image. The blue color box and purple color box are used respectively to contrast the
609 clean day and the polluted day.

610

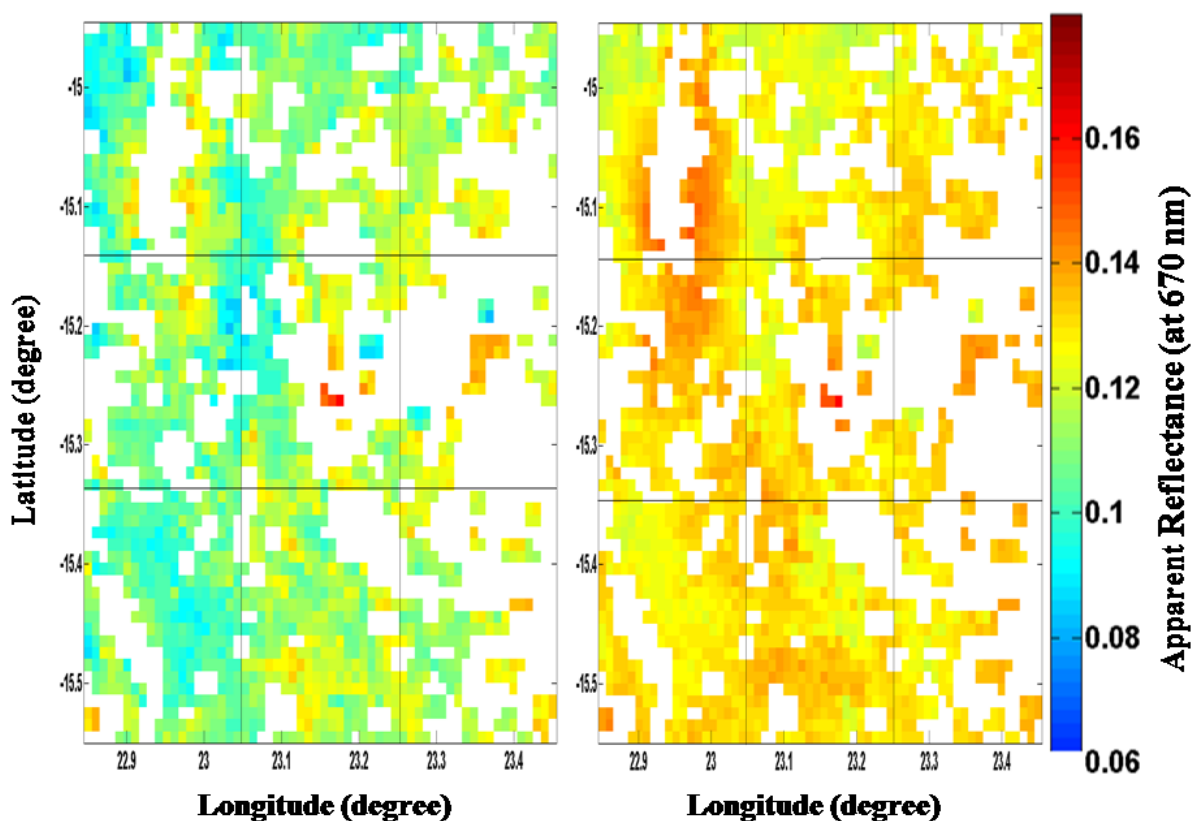


611

612

613 FIG.2. Projected apparent reflectance for the polluted and clean day at 670 nm after applying a
614 common cloud mask to both days. The image on the left shows the reflectance in the blue color
615 box in Fig.1 with an average AOD (at 670 nm) =0.36. The image on the right shows the
616 reflectance in the purple color box in Fig.1 with an averaged AOD (at 670 nm) =0.7. The color
617 bar represents the apparent reflectance.

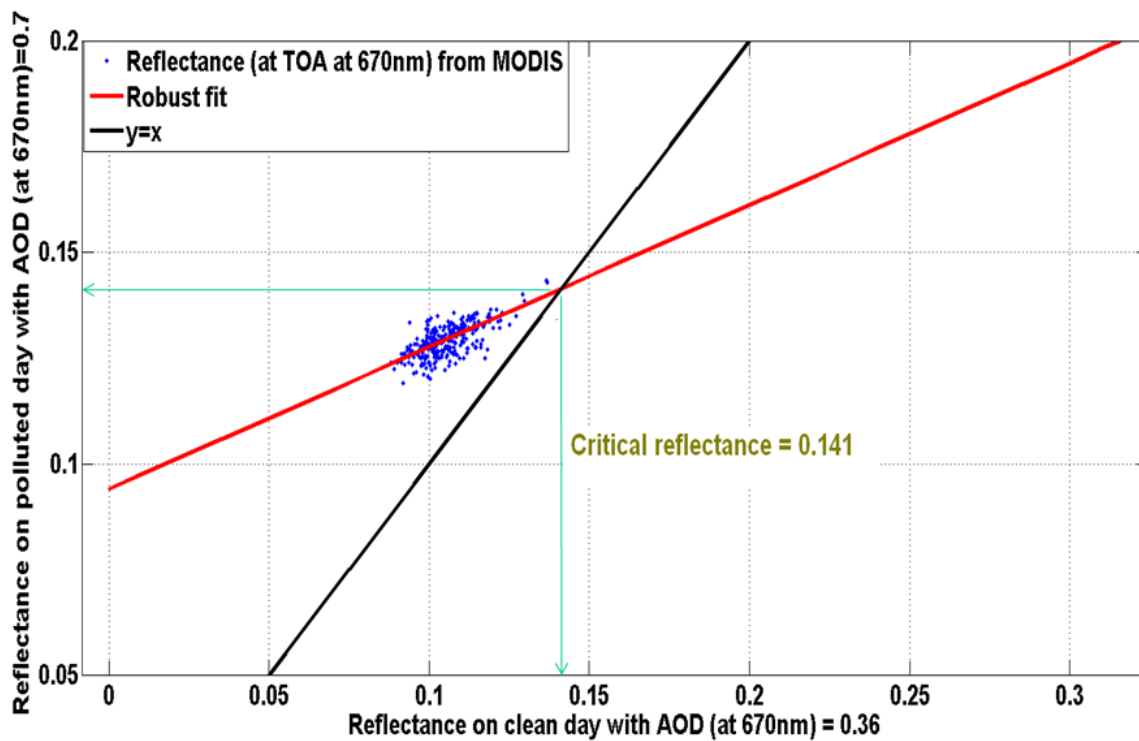
618



619

620

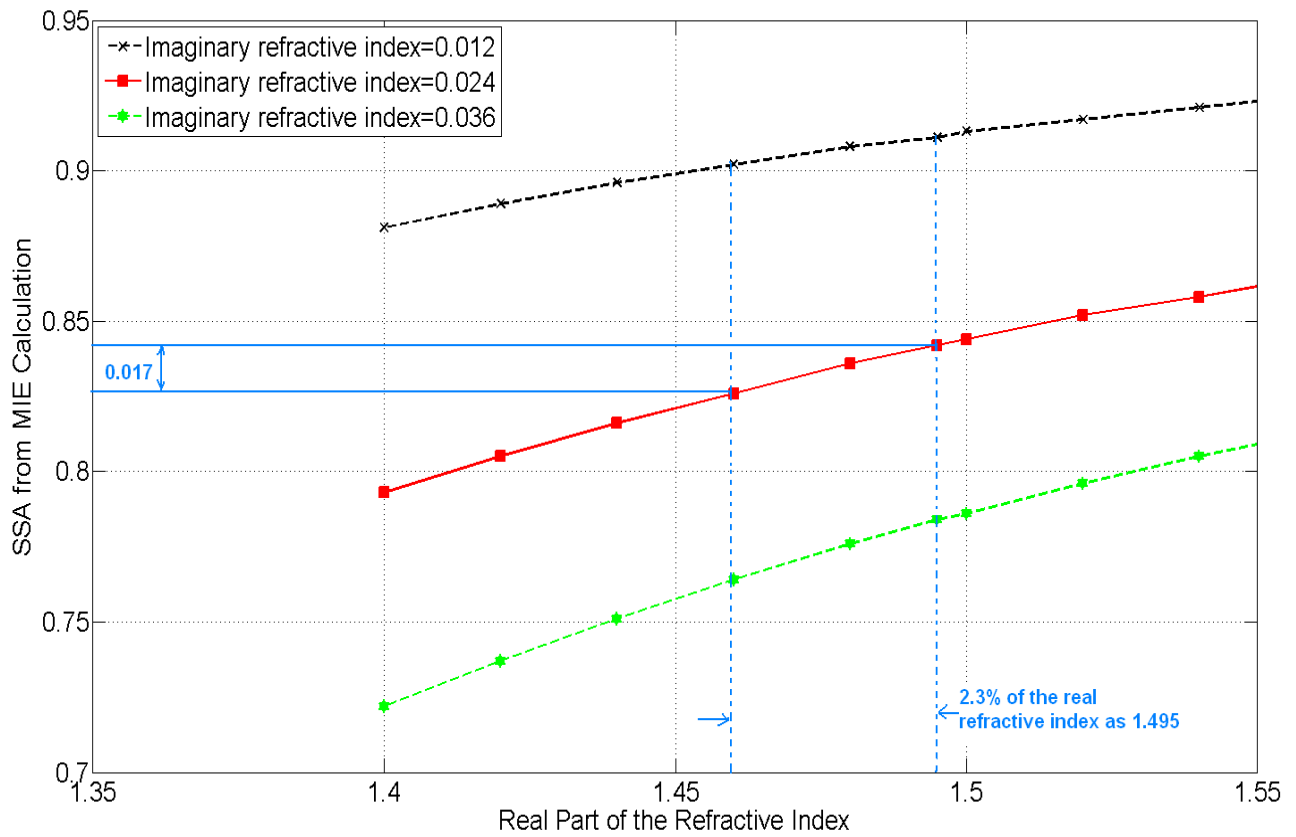
621 FIG.3. This figure demonstrates how to calculate critical reflectance using MODIS data from
622 two days. The blue dots are the scatter plot of the reflectance from the first cell (20×20 km
623 range) on the polluted day (the y-axis) versus that on the clean day (the x-axis). The red color
624 line represents the robust fit of the data. The black color line represents $y=x$, when reflectance
625 (at the TOA) on the clean day equals reflectance (at the TOA) on the polluted day. The
626 reflectance value at the crossing point (as shown by the arrows in the figure) between the black
627 color line and the red color line is defined as “critical reflectance”. The intercept of the fitted red
628 color line on the y- axis is defined as “effective path radiance”.



629

630

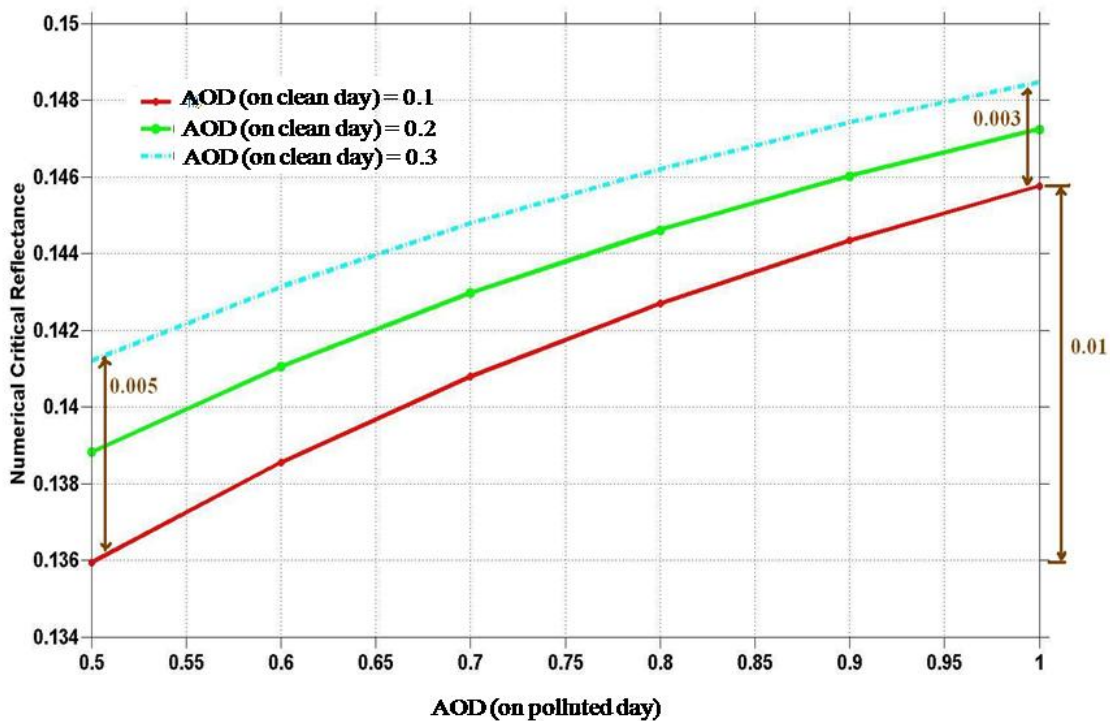
631 FIG.4. Sensitivity study for the variation of the real part of aerosol refractive index. The x- axis
 632 represents the real part of the refractive index, and the y-axis represents aerosol SSA calculated
 633 from Mie theory. The real refractive index as 1.49, the imaginary refractive index as 0.024, and
 634 the input size distribution are from AERONET retrieval results over Mongu on day 250 in year
 635 2000. This result shows that an uncertainty of real part of aerosol refractive index of 2.3% leads
 636 to an SSA uncertainty of 0.01, 0.017, and 0.021 when the imaginary refractive index is 0.012,
 637 0.024, and 0.036 respectively.



638

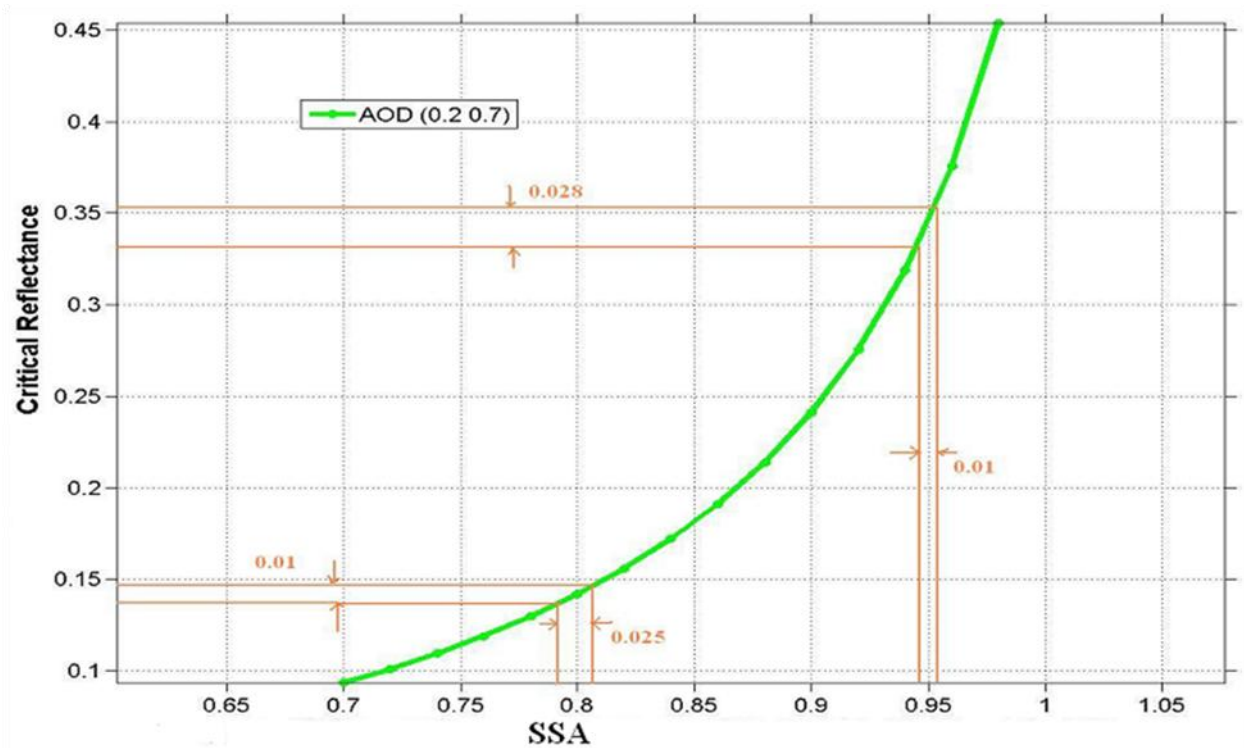
639

640 FIG.5. This figure shows the AOD dependence of the critical reflectance. The x-axis represents
 641 AOD (at 670 nm) on a polluted day, and the y- axis represents the calculated critical reflectance
 642 for AOD values (at 670 nm; on a clean day) of 0.1 (red solid line), 0.2 (green solid line), and 0.3
 643 (continued light blue line). The simulations use the following conditions: solar zenith angle
 644 (SZA)=26.8 degrees, solar azimuth angle (SAZA)=37.77 degrees, detector zenith angle
 645 (DZA)=38.65 degrees, user azimuth angle (phi)=277.38 degrees, wavelength=0.67 μm , and
 646 SSA=0.8. When AOD on the clean day varies from 0.1 to 0.3, the variation of critical reflectance
 647 is 0.005 (AOD of 0.5 on polluted day) and 0.003 (AOD of 1 on polluted day). In addition, when
 648 AOD on the polluted day varies from 0.5 to 1, the variation of critical reflectance is 0.01 (AOD of
 649 0.1 on the clean day).



650
 651

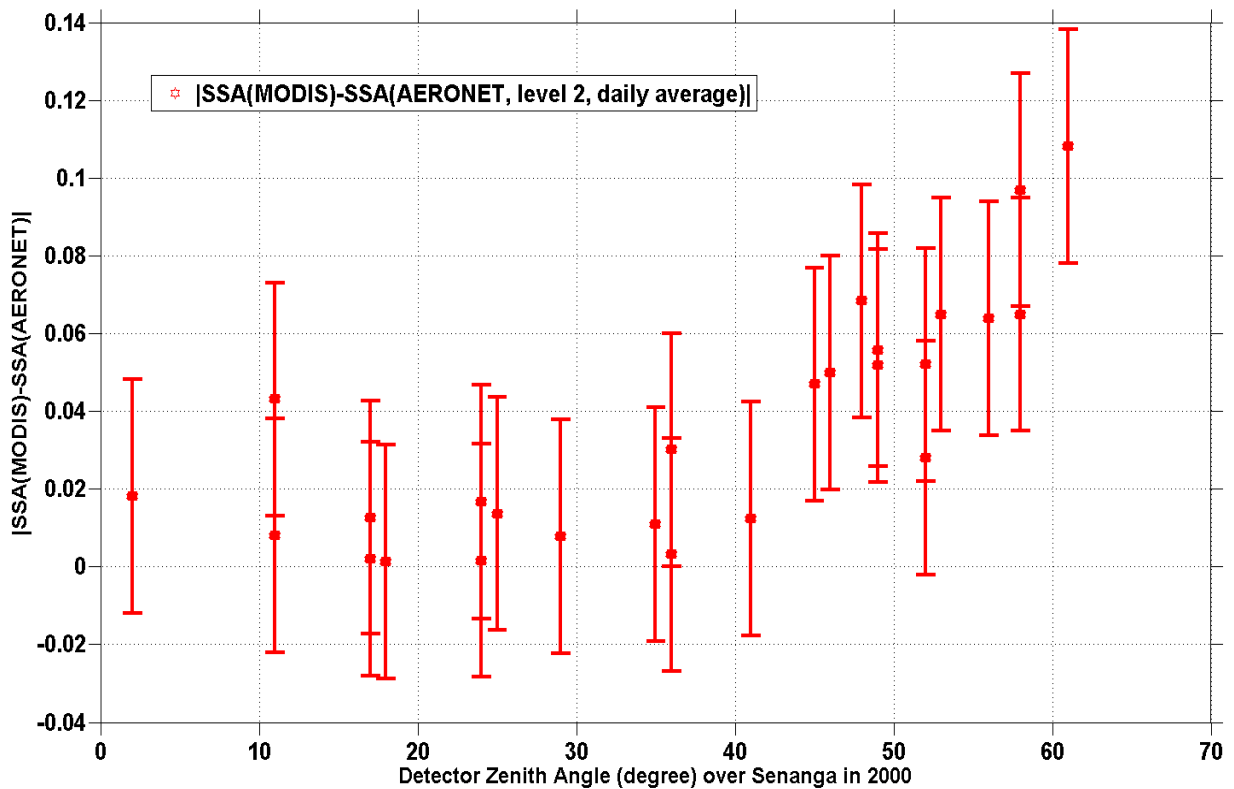
652 FIG.6. The sensitivity study of aerosol SSA (at 670 nm) to varying critical reflectance. The x-
 653 axis represents SSA, and the y-axis represents critical reflectance. The green curve shows the
 654 unique correlation between critical reflectance and SSA. AOD on the clean (polluted day) day is
 655 0.2 (0.7). It shows that the critical reflectance uncertainty of 0.01 leads to an SSA uncertainty of
 656 0.025 (when SSA=0.8). Similarly, a critical reflectance uncertainty of 0.028 causes an SSA total
 657 uncertainty of 0.01 (when SSA=0.95).



658

659

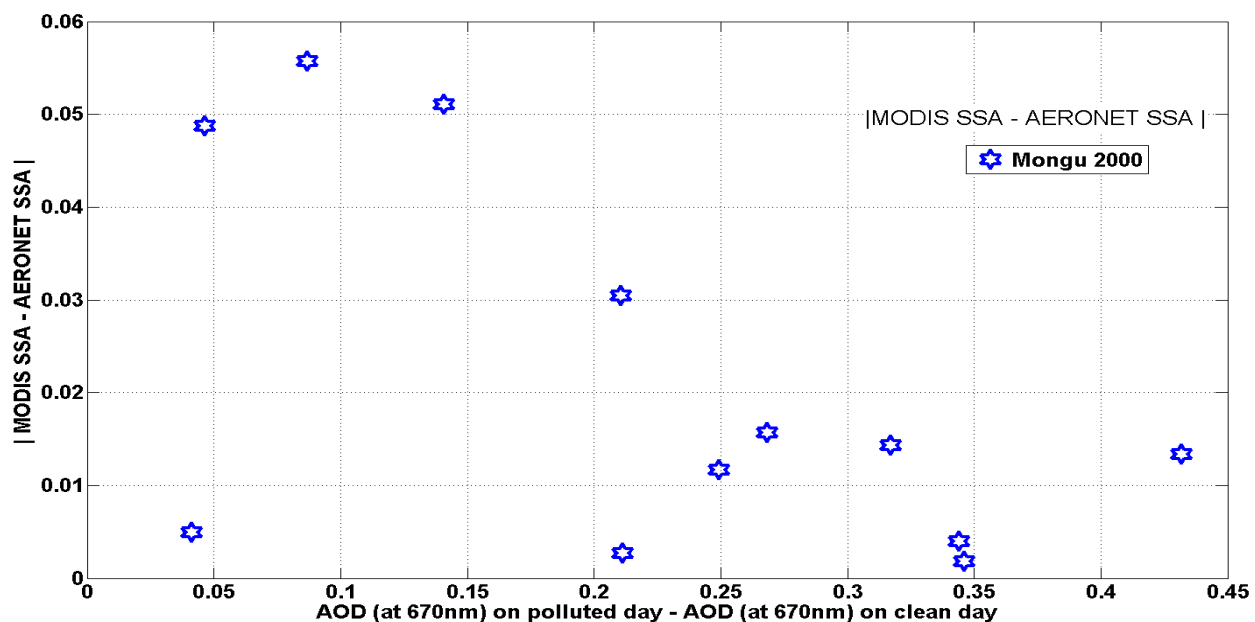
660 FIG.7. This figure demonstrates that DZA affects aerosol SSA retrievals. The x-axis represents
661 DZA for each case, and the y-axis represents the absolute difference between the retrieved
662 aerosol SSA (over Senanga in 2000) from MODIS on *TERRA* and AERONET level 2 daily-
663 averaged aerosol SSA. The red color bar over each data point represents the AERONET SSA
664 uncertainty of 0.03. The result indicates that the difference between aerosol SSA retrieved from
665 MODIS and from AERONET increases as DZA increases. This effect is likely caused by the
666 simplified assumption of a Lambertian surface reflectance in the radiative transfer simulations.



667

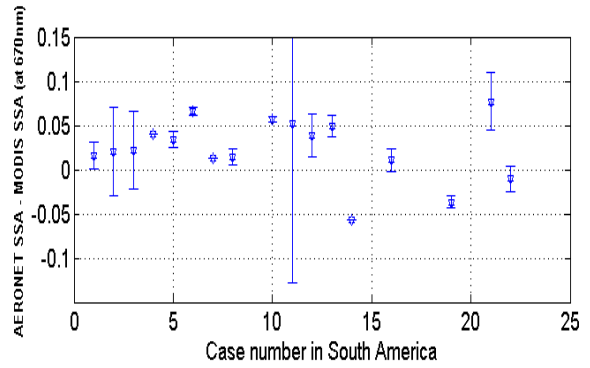
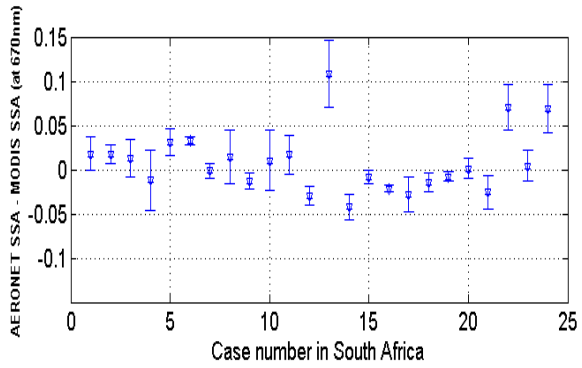
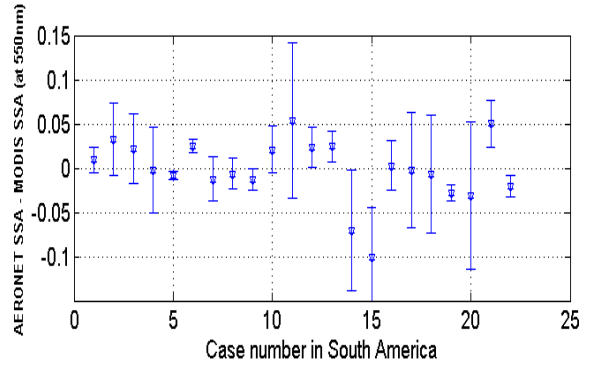
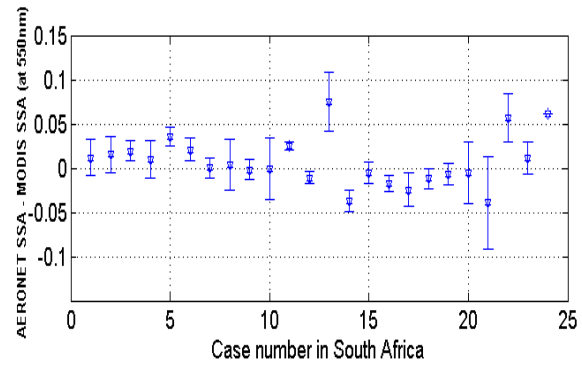
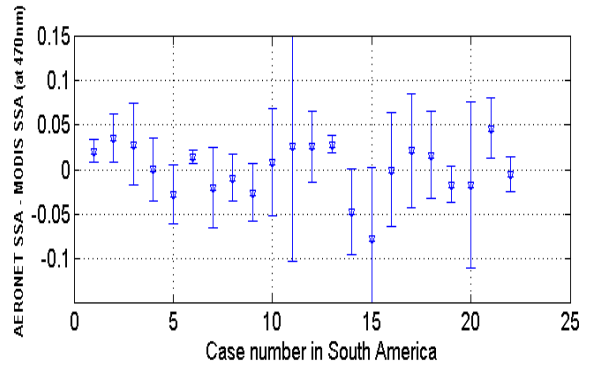
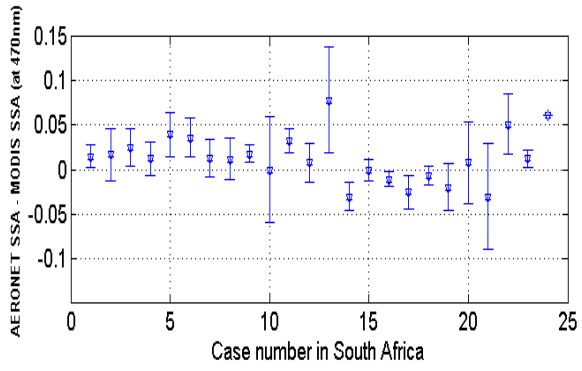
668

669 FIG.8. This figure demonstrates that AOD differences affect aerosol SSA retrievals. The x-axis
670 represents the AOD difference at 670 nm between the clean day and the polluted day, and the y-
671 axis represents the absolute difference between aerosol SSA (over Mongu in 2000) retrieved
672 from MODIS and AERONET level 2 daily-averaged aerosol SSA. The result shows that AOD
673 difference needs to be greater than 0.2 in order to produce a high enough signal to noise ratio and
674 to keep the deviation of MODIS SSA from AERONET SSA below 0.03.



675
676

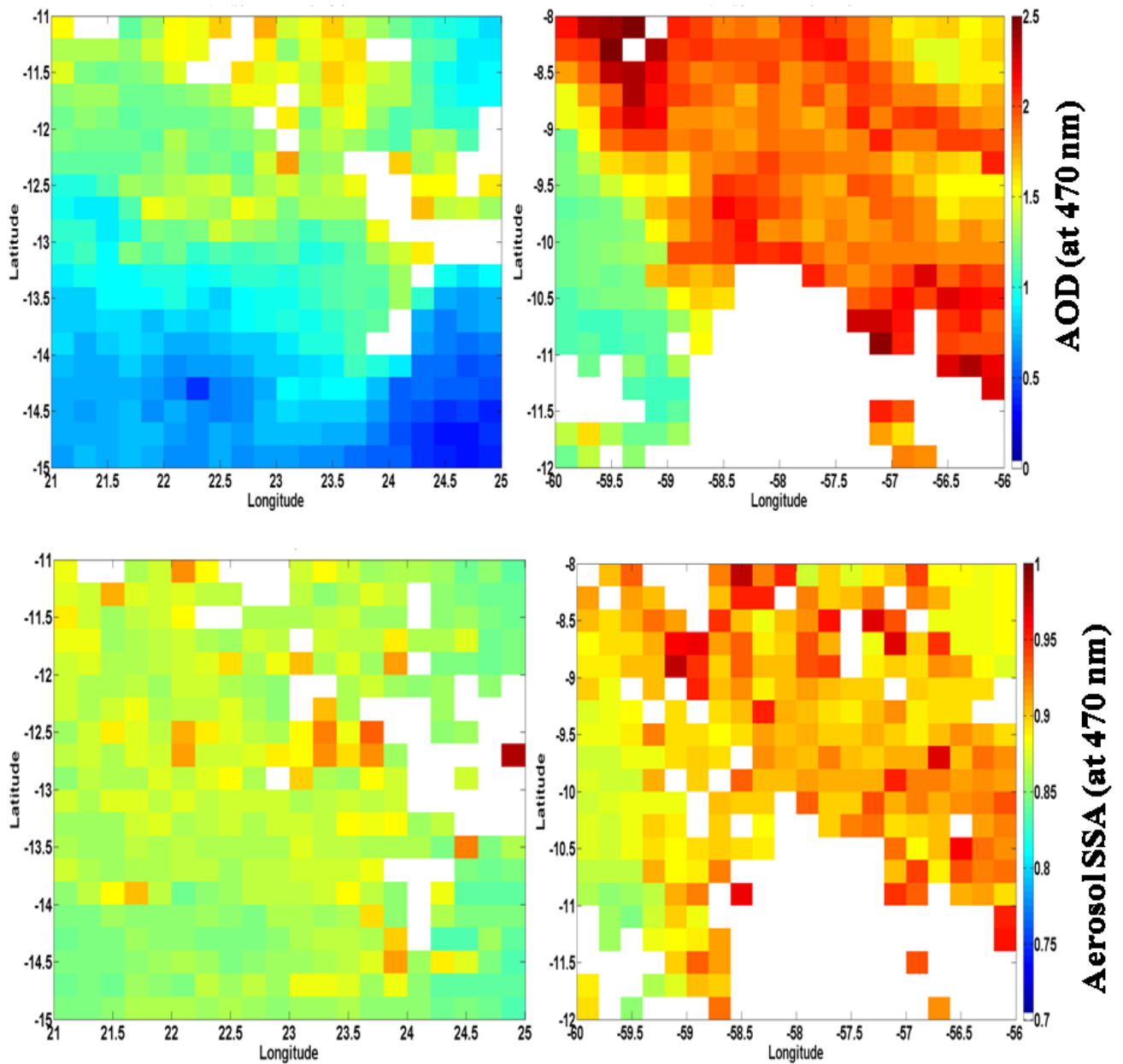
677 FIG.9. Comparison of aerosol SSA retrieved from MODIS with collocated AERONET
678 measurement in South Africa (plots on the left) and South America (plots on the right). The x-
679 axis represents the case numbers, and the y-axis represents the difference between aerosol SSA
680 from AERONET and from MODIS. In addition, bars over each data point represent SSA
681 variance (among the remaining cells in 60×60 km range) at a 50% of confidence interval and
682 with a chi square distribution correction. Since AERONET SSA has an uncertainty of 0.03, the
683 aerosol SSA retrieved from MODIS agrees well with AERONET measurements (68% by only
684 considering the mean; 88% by considering the mean and the variance), i.e., the absolute
685 difference between aerosol SSA from AERONET and MODIS is smaller than 0.03. The result
686 also shows that aerosol SSA has a larger spatial variation in South America than in South Africa.



687

688

689 FIG. 10. Regional AOD and aerosol SSA (at 470 nm) maps. The figures on the left represent the
690 region over South Africa with latitude = [-15 to -11] and longitude = [21 to 25] on day 254 in
691 2000 (day 238 as the clean day). The figures on the right represent the region over South
692 America with latitude = [-12 to -8] and longitude = [-60 to -56] on day 241 in 2006 (with 225 as
693 the clean day). Both images have a resolution of 20×20 km.

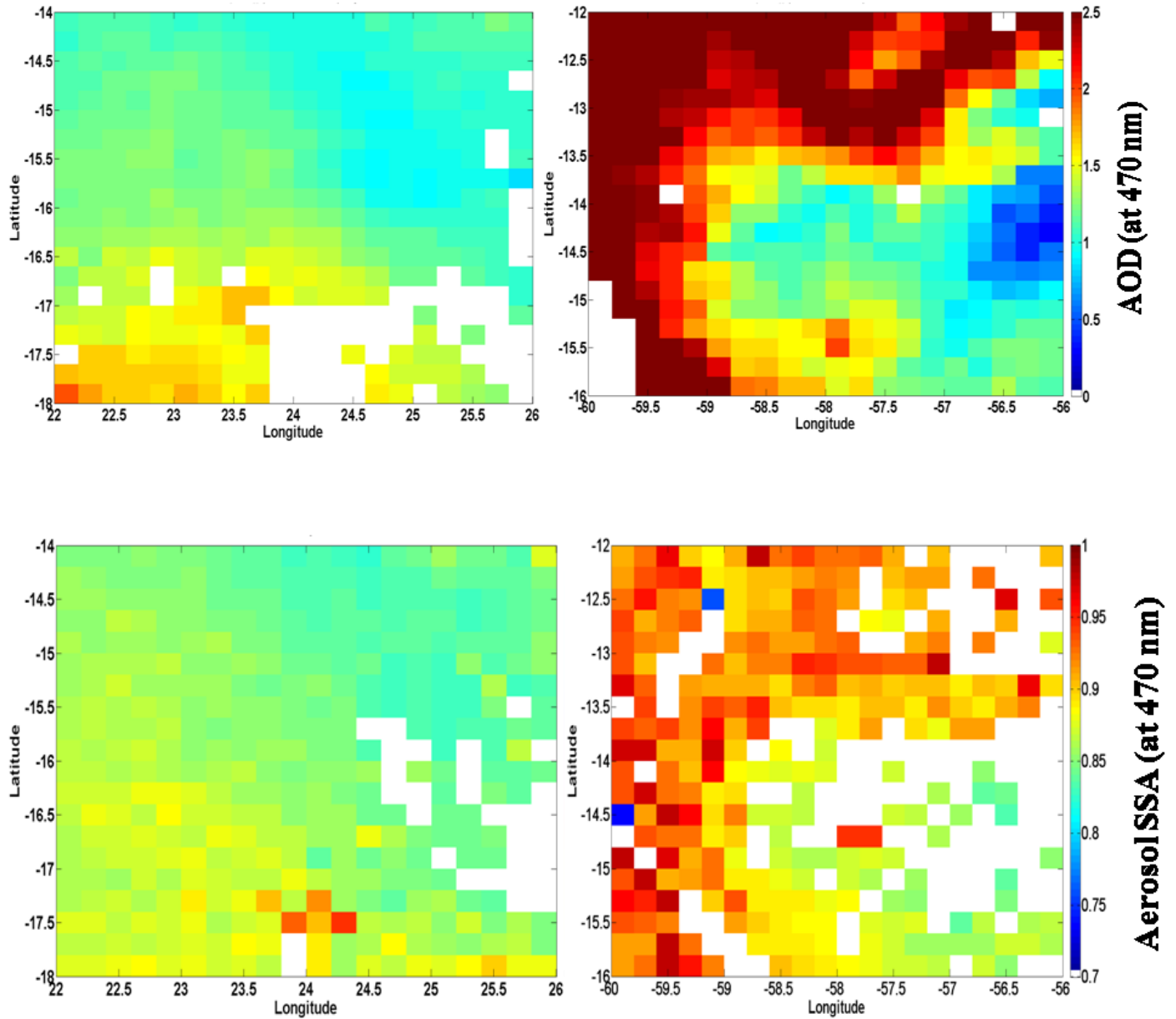


694

695

696

697 FIG. 11. Regional AOD and aerosol SSA (at 470 nm) maps. The figures on the left represent the
698 region over South Africa with latitude = [-18 to -14] and longitude = [22 to 26] on day 250 in
699 2000 (day 266 as the clean day). The figures on the right represent the region over South
700 America with latitude = [-16 to -12] and longitude = [-60 to -56] on day 252 in 2004 (with 268 as
701 the clean day). Both images have a resolution of 20×20 km.



702

703

704